

## Origin of Traveling Rolls in Electroconvection of Nematic Liquid Crystals

Michael Dennin,<sup>1</sup> Martin Treiber,<sup>2</sup> Lorenz Kramer,<sup>2</sup> Guenter Ahlers,<sup>1</sup> and David S. Cannell<sup>1</sup>

<sup>1</sup>*Department of Physics and Center for Nonlinear Science, University of California at Santa Barbara, Santa Barbara, California 93106*

<sup>2</sup>*Physikalisches Institut der Universität Bayreuth, D-95440 Bayreuth, Germany*

(Received 3 May 1995)

Electroconvection in nematic liquid crystals exhibits a Hopf bifurcation to traveling rolls for a wide parameter range. The model normally used to describe electroconvection fails to predict this. A recent theoretical extension, the weak-electrolyte model, incorporates the dissociation-recombination reaction of the ionic dopant in the sample and does predict a Hopf bifurcation for a range of parameter values. We present a quantitative experimental test of this theory using the nematic liquid crystal I52. Measured Hopf frequencies at the onset of convection agree well with the theory.

PACS numbers: 83.70.Jr, 47.20.Ky, 47.65.+a

Electroconvection (EC) in nematic liquid crystals (NLC) is a paradigm for pattern formation in anisotropic systems [1–4]. An EC cell consists of a NLC doped with ionic impurities and confined between glass plates which are coated with transparent electrodes and treated to produce uniform planar (parallel to the plates) alignment of the director  $\hat{\mathbf{n}}$  (the average molecular orientation). At a critical value  $V_c$  of an applied ac voltage amplitude, fluctuations in the anisotropic conductivity resulting from fluctuations of  $\hat{\mathbf{n}}$  generate a local charge density sufficient to drive a transition from a uniform state to a state with spatial variation (Carr-Helfrich mechanism) [5]. A great variety of spatiotemporal structures is observed, including rolls [6,7], traveling waves [7–12], defect chaos [9,13], and chaos at onset [12].

In a theory of EC, the equations for the velocity field, the director field, the charge density, and the electric field require at least 14 parameters [5]. Nonetheless, a detailed linear stability analysis [2] of the model originally introduced by Helfrich [14] and subsequently developed by a number of authors (see Ref. [5] and references therein) quantitatively predicts both  $V_c$  and the initial wave vector of the pattern. However, this model, which we will refer to as the standard model (SM), fails to predict the traveling-roll states (Hopf bifurcation), which are observed experimentally [7–12]. A number of *possible* reasons have been suggested, including imperfect director alignment and conductivity effects [2,3]; however, until the recently introduced generalization of the SM, the weak-electrolyte model (WEM) [15], no detailed theory has predicted the existence of traveling rolls in EC.

In the SM, the dynamics of the velocity and director fields are governed by a generalized Navier-Stokes equation and by equations for the director [2,5]. The dynamics of the charge density is governed by the continuity equation with the charge and current densities related to the electric field by Gauss' law and Ohm's law. Experimental work on EC [11] using the NLC *4-ethyl-2-fluoro-4'-[2-(trans-4-pentylcyclohexyl)-ethyl] biphenyl* (I52) has shown that the conductivity is not frequency independent

as assumed. The WEM incorporates into the SM dissociation and recombination of the dopant [16,17], and its effects on the conductivity. These WEM effects are also known to exist in other NLC's [18].

The WEM reproduces the experimentally observed dependence of the frequency  $\omega$  of the pattern on the anisotropy  $\epsilon_a = \epsilon_{\parallel} - \epsilon_{\perp}$  of the dielectric constant, the conductivity, and the cell thickness  $d$ . The WEM includes a competition of two fields with different intrinsic time scales, which is a common mechanism of Hopf bifurcations in pattern-forming systems [19,20]. The success of the WEM in explaining the *linear* properties of our system is especially important because there is a continuous oscillatory instability to spatiotemporal chaos [12]. In principle, it is possible to derive *nonlinear* coupled complex Ginzburg-Landau equations from the WEM and to compare their spatiotemporal properties with the observed [12] spatiotemporal complexity. Usually this is not possible for chaotic systems [21] because the primary bifurcation is backwards, because chaos occurs only after secondary bifurcations, or because the system size accessible to experiments is too small.

In the WEM, there are two ionic charge carriers with charges  $\pm e$  [16], which are coupled through a dissociation-recombination reaction for their number densities  $n^+(\mathbf{x}, t)$  and  $n^-(\mathbf{x}, t)$  [17], and the ionic species have constant, possibly different, mobility tensors  $\mu^{\pm}$  with principal values perpendicular and parallel to  $\hat{\mathbf{n}}$ ,  $\mu_{\perp}^{\pm}$ , and  $\mu_{\parallel}^{\pm}$ , respectively. The  $\mu_{(\perp,\parallel)}^{\pm}$  are defined in terms of the ion's steady-state velocities in a quiescent fluid with an applied electric field,  $v_{(\perp,\parallel)}^{\pm} = \mu_{(\perp,\parallel)}^{\pm} E_{(\perp,\parallel)}$ . The ratio  $\mu_{\parallel}/\mu_{\perp}$  is assumed to be the same for both species. The WEM expresses the total space-charge density  $\rho(\mathbf{x}, t)$ , which already appears in the SM as  $\rho(\mathbf{x}, t) = e[n^+(\mathbf{x}, t) - n^-(\mathbf{x}, t)]$ . Unlike for the SM, the local conductivity tensor is an additional variable with components given by  $\sigma_{ij}(\mathbf{x}, t) = \sigma(\mathbf{x}, t)[\delta_{ij} + n_i n_j (\mu_{\parallel}/\mu_{\perp} - 1)]$ , where  $n_i$  are the director components and  $\delta_{ij}$  is the Kronecker delta function. Here  $\sigma(\mathbf{x}, t) = e[\mu_{\perp}^+ n^+(\mathbf{x}, t) + \mu_{\perp}^- n^-(\mathbf{x}, t)]$ .

The WEM consists of two equations which couple  $\sigma(\mathbf{x}, t)$  and  $\rho(\mathbf{x}, t)$  plus the SM equations for  $\hat{\mathbf{n}}$  and fluid velocity  $\mathbf{v}$ . The new equations for  $\sigma$  and  $\rho$  are given in Ref. [15], and the SM equations are in Ref. [2]. The charge density is coupled to  $\hat{\mathbf{n}}$  and  $\mathbf{v}$  as in the SM, and  $\sigma(\mathbf{x}, t)$  couples to  $\hat{\mathbf{n}}$  and  $\mathbf{v}$  via the conductivity tensor and the advection term. The boundary conditions in the experiment are unknown, but using the frequency dependence of the capacitance we determined experimentally that the thickness of the charged boundary layers at the electrodes is small compared to  $d$ . In this limit, the model is insensitive to the boundary conditions [15].

The SM has two relevant time scales: a charge-relaxation time  $\tau_q = \epsilon_0 \epsilon_{\perp} / \sigma_{\perp}$  and the director-relaxation time  $\tau_d = \gamma_1 d^2 / K_{11} \pi^2$ . Here  $\epsilon_{\perp}$  is the principal value of the dielectric-constant tensor perpendicular to  $\hat{\mathbf{n}}$ ,  $\gamma_1$  is a typical viscosity,  $K_{11}$  is an orientational elastic constant, and  $\sigma_{\perp}$  and  $\sigma_{\parallel}$  are the equilibrium principal values of the conductivity tensor. Typically,  $\tau_d$  is  $\mathcal{O}(1 \text{ s})$  and  $\tau_q$  is  $\mathcal{O}(10^{-3} \text{ s})$ . The WEM has two additional time scales: a recombination time  $\tau_{\text{rec}} = 1/(2k_r n_0)$  for the dissociation-recombination reaction and a migration time  $\tau_{\text{mig}} = d^2 / \pi^2 (\mu_{\perp}^+ + \mu_{\perp}^-) V^{(0)}$  for a charge to traverse the cell under an applied voltage  $V^{(0)}$  which is of the order of the critical voltage for low external frequencies. Here  $k_r$  is the recombination rate of the ions,  $n_0$  is the equilibrium number density of either species of ions, and  $V^{(0)} = \pi [K_{11} / (\tau_q \sigma_a)]^{1/2}$ , with  $\sigma_a = \sigma_{\parallel} - \sigma_{\perp}$ . The SM is recovered in the limit of  $\tau_{\text{rec}} / \tau_q \rightarrow 0$  and  $\tau_{\text{mig}} / \tau_q \rightarrow \infty$ .

In Ref. [15] the WEM was applied to rolls with their axes perpendicular to  $\hat{\mathbf{n}}$  (normal rolls). For quantitative comparison with the present experiment, we applied it to the more general case of rolls with a nonzero angle  $\Theta$  between their wave vectors and the undistorted director (oblique rolls), where one also has  $y$  components of  $\hat{\mathbf{n}}$  and the velocity field which are already predicted by the SM. With  $z$  perpendicular to the electrodes and  $x$  parallel to the undistorted  $\hat{\mathbf{n}}$ , the fields of the WEM were expanded using a Galerkin expansion in  $z$  and a Fourier mode with wave numbers  $q$  and  $p$  in the  $x$  and  $y$  directions, respectively. Proceeding as in [15], we arrive at an autonomous set of three ordinary differential equations (ODE's) in (slow) time with real coefficients for the amplitude of the local deviation of the conductivity from its equilibrium value,  $A_{\sigma}(t)$ , and for the amplitudes of the lowest-order mode in the Galerkin expansion of the Fourier mode of the  $z$  and  $y$  components of  $\hat{\mathbf{n}}$ ,  $n_z^{(0)}(t)$ , and  $n_y^{(0)}(t)$ , respectively. The critical SM mode  $A_n(t)$  is a linear combination of  $n_z^{(0)}(t)$  and  $n_y^{(0)}(t)$ , and near threshold, the three ODE's can be further reduced systematically (restricting to the linear part) to a  $2 \times 2$  normal form for  $A_{\sigma}(t)$  and  $A_n(t)$  given by

$$\begin{aligned} \dot{A}_{\sigma} &= \lambda_{\sigma}(R) A_{\sigma} - \tilde{\alpha}^2 R \sigma_a^{(\text{eff})} (\sigma_{\perp} \tau_d)^{-1} A_n, \\ \dot{A}_n &= \frac{R \sigma_{\perp}}{\sigma_a^{(\text{eff})} \tau_d} \left( \frac{C}{1 + (\beta \Omega \tau_q)^2} \right)^2 A_{\sigma} + \lambda_n(R) A_n, \end{aligned} \quad (1)$$

where  $R = (V/V^{(0)})^2$  is the control parameter and  $\Omega$  the angular frequency of the applied voltage. The diagonal coefficients  $\lambda_{\sigma}(R) = -\tau_q^{-1} - \tau_d^{-1} (R \tilde{\alpha}^2 \beta) / [1 + (\beta \Omega \tau_q)^2] < 0$  and  $\lambda_n(R) = \epsilon / \tau_0^{\text{SM}}$  are the growth rates of the  $\sigma$  mode and the SM amplitude, respectively. Here  $\epsilon = R/R_c - 1$  is the relative distance from threshold  $R_c$ ,  $\tau_0^{\text{SM}}$  is the correlation time of the SM amplitude equation [ $\mathcal{O}(\tau_d)$ ], and  $\beta = [(1 + \epsilon_a / \epsilon_{\perp})(q_c d)^2 + (p_c d)^2 + 1] / [(1 + \sigma_a / \sigma_{\perp})(q_c d)^2 + (p_c d)^2 + 1] \approx 0.85$ . The dimensionless quantity  $C$  contains only SM quantities [15] and is of order unity for our experiments [22]. The effective conductivity anisotropy  $\sigma_a^{(\text{eff})} \approx \sigma_a [\beta - \epsilon_a \sigma_{\perp} / \sigma_a \epsilon_{\perp}] / [1 + (\beta \Omega \tau_q)^2]$  is proportional to the charge produced by the Carr-Helfrich mechanism [5]. The decisive coupling which provides the Hopf mechanism is proportional to  $\tilde{\alpha}^2 = \mu_{\perp}^+ \mu_{\perp}^- \gamma_1 \pi^2 / \sigma_a d^2$ . It drives  $A_{\sigma}$  negative as  $A_n$  grows, with the result that  $A_{\sigma}$  acts to retard the growth of  $A_n$ .

There are two main predictions of the WEM. For sufficiently high mobilities and small recombination rates, there is a nonzero Hopf frequency  $\omega$  at threshold (the imaginary part of the growth rate of the  $2 \times 2$  equations is nonzero for zero real part),  $\omega = \tilde{\omega} \sqrt{1 - [\lambda_{\sigma}(R_c) / \tilde{\omega}]^2}$ , where

$$\tilde{\omega} = C \left( \frac{\pi}{d} \right)^3 \frac{R_c K_{11}}{1 + (\beta \Omega \tau_q)^2} \sqrt{\frac{\mu_{\perp}^+ \mu_{\perp}^-}{\gamma_1 \sigma_a}}. \quad (2)$$

There is an upward shift of  $R_c$  relative to the SM prediction. For nonzero  $\omega$ , the shift is

$$\Delta \epsilon = \frac{R_c - R_c^{\text{SM}}}{R_c^{\text{SM}}} = -\tau_0^{\text{SM}} \lambda_{\sigma}(R_c), \quad (3)$$

which is generally less than 1%. Within the accuracy of the measured material parameters, the WEM predicts the SM values for  $V_c$  and  $\Theta$  which generally agree with experiment [2].

The apparatus [11] consisted of a computer-controlled imaging system, temperature-control stage with a stability of  $\pm 1 \text{ mK}$  and range up to  $60 \text{ }^{\circ}\text{C}$ , and electronics for applying the ac voltage and measuring the conductivity of the cells. The voltage amplitude ranged up to  $40 \text{ V}$  at a frequency  $\Omega/2\pi$  from  $10$  to  $200 \text{ Hz}$ . Planar alignment was obtained with a rubbed polyimide film which was spin coated onto the transparent electrodes of indium-tin oxide. The I52 was doped with 2% by weight molecular iodine [23]. Usually,  $d$  was  $28 \pm 2 \text{ } \mu\text{m}$ , uniform to  $\pm 0.5 \text{ } \mu\text{m}$ . The frequency dependence of the measured conductivities was consistent with predictions of the WEM [24].

We measured the critical voltage  $V_c$ , the angle  $\Theta$  between the wave vector and the undisturbed  $\hat{\mathbf{n}}$ , and the Hopf frequency  $\omega$  as a function of  $\Omega$ . The  $\epsilon$  resolution was  $0.001$ . For each  $\epsilon$ ,  $\omega$  was determined from a time series of small ( $9d \times 9d$  about  $2.5\tau_d$  apart) images, and a larger ( $46d \times 46d$ ) image was used to measure  $\Theta$ . For each single image we computed the spatial power spectrum  $S(\mathbf{k})$ , and for each time series we computed  $S(\mathbf{k}, \omega)$ .

For  $S(\mathbf{k})$ , there were two pairs of peaks corresponding to coexisting zig and zag rolls (states with angle  $\theta$  and  $\pi - \theta$ , respectively). For  $S(\mathbf{k}, \omega)$ , there were four pairs of peaks corresponding to right- and left-traveling zig and zag rolls. We averaged  $\Theta = \tan^{-1}(p/q)$  of the two modes, where the components  $q$  and  $p$  of  $\mathbf{k}$  were determined from the first moment of the relevant peak in  $S(\mathbf{k})$ . We used the average  $\omega$  of the four degenerate traveling rolls computed from an average of the relevant peaks in  $S(\mathbf{k}, \omega)$ .

We determined  $V_c$  using the total power under the relevant pairs of peaks in  $S(\mathbf{k})$  and  $S(\mathbf{k}, \omega)$ . The transition is forward, i.e., nonhysteretic and continuous [12], and  $S(\mathbf{k})$  and  $S(\mathbf{k}, \omega)$  yielded the same results for  $V_c$ . Both  $\Theta$  and  $\omega$  were determined as a function of  $\epsilon$ , and the value obtained by extrapolating to  $\epsilon = 0$  was compared with theory.

A meaningful test of the WEM requires knowledge of the following SM parameters: the three elastic constants ( $K_{11}, K_{22}, K_{33}$ ), six viscosities ( $\alpha_1, \alpha_2, \alpha_3, \alpha_4, \alpha_5, \alpha_6$ ),  $\sigma_{\perp}, \sigma_{\parallel}, \epsilon_{\perp}, \epsilon_{\parallel}$ , and  $d$ . In addition, two new parameters  $\sqrt{\mu_{\perp}^+ \mu_{\perp}^-}$  and  $\lambda_{\sigma}(R_c)$  are needed. The requirement that the WEM recovers the correct SM prediction for  $V_c$  and  $\Theta$  sets an upper limit on  $\lambda_{\sigma}(R_c)$  from  $|\lambda_{\sigma}(R_c)|\tau_0^{\text{SM}} \ll 1$ . The SM parameters were all determined [25] from literature values, independent measurements, and by fitting our results for  $V_c$  and  $\Theta$  for all six temperatures. Typical examples of the fits are shown in Fig. 1.

Both  $\tau_0^{\text{SM}}$  and  $2\pi/\tilde{\omega}$  are  $\mathcal{O}(1 \text{ s})$ , so  $|\lambda_{\sigma}(R_c)|\tau_0^{\text{SM}} \ll 1$  implies  $[\lambda_{\sigma}(R_c)/\tilde{\omega}]^2 \ll 1$ . Therefore,  $\omega \approx \tilde{\omega}$  and is computed using Eq. (2) with only one adjustable parameter,  $\sqrt{\mu_{\perp}^+ \mu_{\perp}^-}$  [25], for each temperature. The increased discrepancy (up to 15%) at the lower temperatures

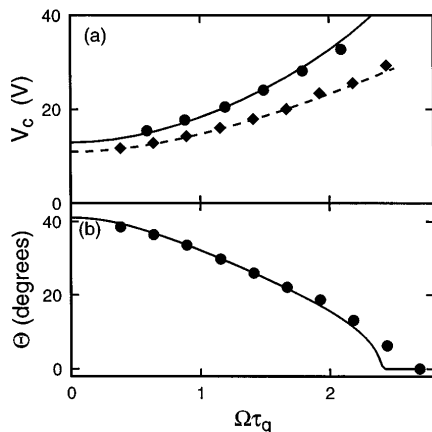


FIG. 1. Critical rms voltage amplitude  $V_c$ , and angle  $\Theta$  of the wave vector with respect to  $\hat{\mathbf{n}}$ , as a function of the dimensionless applied frequency  $\Omega\tau_q$ . Here  $\tau_q = \epsilon_0\epsilon_{\perp}/\sigma_{\perp}$ . (a)  $V_c$  for  $T = 30^\circ\text{C}$  (circles, solid line) and  $45^\circ\text{C}$  (diamonds, dashed line). The symbols (lines) are the experimental (theoretical) result. The  $\Omega\tau_q \rightarrow 0$  limit is used to determine the temperature dependence of  $\sigma_a/\sigma_{\perp}$  [25]. (b)  $\Theta$  for  $T = 45^\circ\text{C}$ . The temperature dependence of  $\Theta$  is relatively weak.

[Fig. 2(a)] is related primarily to experimental uncertainties in the very small measured conductivity. For most of the data, experiment and theory agree to within 5% of  $\omega$ . Since the SM prediction is  $\omega = 0$  [not shown on the scale used in Figs. 2(a) or 2(b)], we regard this as quantitative support for the WEM.

The WEM captures a number of features of the experiment which are independent of the uncertainties in the material parameters. Both in the model and in the experiment, the  $\Omega$  dependence of  $\omega$  is determined mostly by  $\epsilon_a$ . For  $\epsilon_a < 0$  ( $T < 60^\circ\text{C}$ )  $\omega$  increases with  $\Omega$ , and for  $\epsilon_a \approx 0$  ( $T = 60^\circ\text{C}$ ) it is essentially constant [see Figs. 2(a) and 2(b)]. In addition, the model predicts  $\omega \propto \sigma_{\perp}^{-1/2}d^{-3}$ . The correct dependence on temperature in Figs. 2(a) and 2(b) reflects the  $\sigma_{\perp}^{-1/2}$  scaling ( $\sigma_{\perp}$  varies by factor of 5 over the temperature range  $30 \leq T \leq 60^\circ\text{C}$ ). Figure 2(c) compares results from a  $28 \mu\text{m}$  cell with those from a  $57 \mu\text{m}$  cell, both at  $50^\circ\text{C}$ . We find the expected scaling with  $d$  for high values of  $\Omega$ . In the WEM, the decrease of  $\omega$  to zero for the thicker cell occurs when  $\tilde{\omega}$  becomes of order  $\lambda_{\sigma}$  and depends on the value of  $\tau_{\text{rec}}$ . Further work is needed to test the theory in this regime, since an extremely fine tuning of  $\tau_{\text{rec}}$  is required to match the experiment.

The evidence presented here strongly supports the conclusion that the WEM has captured the main mechanism of the Hopf bifurcation in EHC which was missing in the SM. In both the models, the charge density (which is

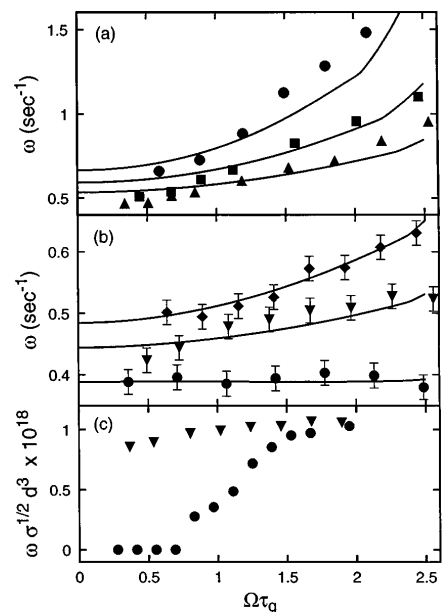


FIG. 2. Hopf frequency  $\omega$  as a function of  $\Omega\tau_q$ . The SM prediction  $\omega = 0$  is well below the bottom of (a) and (b). The abrupt change of slope in the theoretical curves of (a) and (b) corresponds to the Lifshitz point. (a)  $T = 30^\circ\text{C}$  (circles),  $35^\circ\text{C}$  (squares), and  $40^\circ\text{C}$  (triangles). (b)  $T = 45^\circ\text{C}$  (diamonds),  $50^\circ\text{C}$  (triangles), and  $60^\circ\text{C}$  (circles). Lines correspond to the WEM. (c)  $\omega\sigma_{\perp}^{1/2}d^3$  as a function of  $\Omega\tau_q$  for  $d = 28 \mu\text{m}$  and  $\sigma_{\perp} = 8.5 \times 10^{-9} \Omega^{-1} \text{m}^{-1}$  (triangles) and for  $d = 57 \mu\text{m}$  and  $\sigma_{\perp} = 1.1 \times 10^{-8} \Omega^{-1} \text{m}^{-1}$  (circles), both at  $T = 50^\circ\text{C}$ .

proportional to  $A_n$  for  $\tau_q/\tau_d \ll 1$ ) drives the instability via the electrical volume force. As discussed earlier, the coupling of  $A_n$  to  $A_\sigma$  in the WEM provides an additional stabilizing mechanism which is not present in the SM. This stabilizing mechanism is responsible for the Hopf bifurcation provided that the time scale for the feedback is sufficiently slow. The interplay between a primary instability mechanism and a slower stabilizing mechanism seems to be a common feature of pattern-forming systems showing a Hopf bifurcation. In thermal convection in a binary fluid with a negative separation ratio, the concentration field is slow and provides the stabilizing mechanism which counteracts the buoyancy-driven instability [19]. In thermal convection in a NLC with  $\hat{n}$  aligned with the temperature gradient, the slow director field provides the stabilizing mechanism [20].

M. D., G. A., and D. S. C. acknowledge support by the National Science Foundation through Grant No. DMR94-19168. M. T. and L. K. acknowledge support by Deutsche Forschungsgemeinschaft (SFB213, Bayreuth).

- [1] For a recent review of pattern formation in liquid crystals, see L. Kramer and W. Pesch, *Annu. Rev. Fluid Mech.* **27**, 515 (1995).
- [2] E. Bodenschatz, W. Zimmermann, and L. Kramer, *J. Phys. (Paris)* **49**, 1875 (1988); L. Kramer, E. Bodenschatz, W. Pesch, W. Thom, and W. Zimmermann, *Liquid Cryst.* **5**, 699 (1989).
- [3] W. Zimmerman, in *Nematics: Mathematical and Physical Aspects*, edited by J.-M. Coron, J.M. Ghidaglia, and F. Helein, NATO ASI Ser. C, Vol. 332 (Kluwer Academic Publishers, Dordrecht, 1991), p. 401.
- [4] I. Rehberg, B.L. Winkler, M. de la Torre Juárez, S. Rasenat, and W. Schöpf, *Festkörperprobleme* **29**, 35 (1989).
- [5] For a review of the Carr-Helfrich mechanism and the history of EC, see, for instance, W.J.A. Goossens, *Advances in Liquid Crystals*, edited by G.H. Brown (Academic Press, New York, 1978), Vol. 3, p. 1.
- [6] R. Ribotta, A. Joets, and L. Lin, *Phys. Rev. Lett.* **56**, 1595 (1986).
- [7] S. Kai and K. Hirakawa, *Prog. Theor. Phys. Suppl.* **64**, 212 (1978).
- [8] A. Joets and R. Ribotta, *Phys. Rev. Lett.* **60**, 2164 (1988).
- [9] I. Rehberg, S. Rasenat, and V. Steinberg, *Phys. Rev. Lett.* **62**, 756 (1989).
- [10] I. Rehberg, S. Rasenat, M. de la Torre Juárez, and V. Steinberg, *Phys. Rev. Lett.* **61**, 2449 (1988).
- [11] M. Dennin, G. Ahlers, and D.S. Cannell, in *Spatio-Temporal Patterns*, edited by P.E. Cladis and P. Muhoray (Addison-Wesley, Reading, 1994), p. 353.
- [12] M. Dennin, D.S. Cannell, and G. Ahlers, *Mol. Cryst. Liq. Cryst.* **261**, 377 (1995).
- [13] A. Joets, X.D. Yang, and R. Ribotta, *Physica (Amsterdam)* **23D**, 235 (1986).
- [14] W. Helfrich, *J. Chem. Phys.* **51**, 4092 (1969).
- [15] M. Treiber and L. Kramer, *Mol. Cryst. Liq. Cryst.* **261**, 311 (1995).
- [16] R. Chang and J.M. Richardson, *Mol. Cryst. Liq. Cryst.* **28**, 189 (1973).
- [17] R.J. Turnbull, *J. Phys. D* **6**, 1745 (1973).
- [18] G. Brière, R. Herino, and F. Mondon, *Mol. Cryst. Liq. Cryst.* **19**, 157 (1972).
- [19] D.T.J. Hurle and E. Jakeman, *J. Fluid Mech.* **47**, 667 (1971).
- [20] H. Lekkerkerker, *J. Phys. (France) Lett.* **38**, 277 (1977).
- [21] M.C. Cross and P.C. Hohenberg, *Rev. Mod. Phys.* **65**, 851 (1993).
- [22] There is a printing error in Eq. (38) of Ref. [15]. The factor  $1 - (\epsilon_a/\epsilon_q)L_{nn}q^2$  should be replaced by  $L_{nn} - (\epsilon_a/\epsilon_q)q^2$ .
- [23] For concentrations significantly less than 2% I<sub>2</sub>, EC was not observed for applied frequencies above 10 Hz.
- [24] M. Dennin, Ph.D. thesis, Department of Physics, University of California at Santa Barbara, 1995 (unpublished).
- [25] We used previous measurements of the rotational viscosity  $\gamma_1$ , the bulk viscosity  $\eta$ , and  $\epsilon_\perp$  [26].  $\epsilon_a$  and  $K_{33}$  were measured as described in Ref. [11].  $\epsilon_a$  varied linearly from  $-0.056$  for  $T = 25^\circ\text{C}$  to zero for  $T = 63^\circ\text{C}$ , and  $K_{33} = (23 \pm 3) \times 10^{-12}$  N independent of temperature. Known relationships between the viscosities give  $\alpha_2 = \alpha_3 - \gamma_1$  and  $\alpha_5 = \alpha_6 - \alpha_2 - \alpha_3$ . The remaining six viscosities and elastic constants were determined in terms of the known parameters by fitting the measured  $V_c$  and  $\Theta$  curves:  $K_{11} = 0.8K_{33}$ ,  $K_{22} = 0.55K_{33}$ ,  $\alpha_1 = 0.1\gamma_1$ ,  $\alpha_3 = 0.1\gamma_1$ ,  $\alpha_4 = 2\eta$ , and  $\alpha_6 = -0.15\gamma_1$ . The measured values of  $V_c$  at zero frequency require  $\sigma_a/\sigma_\perp = 0.26, 0.30, 0.34, 0.38, 0.42,$  and  $0.45$  for  $T = 30, 35, 40, 45, 50,$  and  $60^\circ\text{C}$ , respectively. At these temperatures and  $V = 5$  V, we measured  $\sigma_\perp = 0.28, 0.37, 0.49, 0.65, 0.85,$  and  $1.41 \times 10^{-8} \Omega^{-1} \text{m}^{-1}$  independent of  $\Omega$  to  $\pm 2\%$  for  $\Omega/2\pi > 25$  Hz. For each  $T \geq 30^\circ\text{C}$ , we determined  $\sqrt{\mu_\perp^+ \mu_\perp^-}$  from the Hopf frequency and found it to increase monotonically with  $T$  from  $0.40 \times 10^{-10}$  m to  $0.47 \times 10^{-10} \text{m}^2 \text{V}^{-1} \text{s}^{-1}$ . The clearing point is  $103.4^\circ\text{C}$  [26].
- [26] U. Finkenzeller, T. Geelhaar, G. Weber, and L. Pohl, *Liq. Cryst.* **19**, 123 (1992).